International Journal of Modern Engineering Research (IJMER)
www.ijmer.com Vol.2, Issue.6, Nov-Dec. 2012 pp-4323-4334 ISSN: 2249-6645

A Novel Three-Phase Three-Leg AC/AC Converter Using Nine IGBTS

Mr. V. Sambasiva Rao[1], Mr. M. Lokya[2], Chalasani Hari Krishna[3]

***Abstract*:** *This paper proposes a novel three-phase nine-switch ac/ac converter topology. This converter features sinusoidal in- puts and outputs, unity input power factor, and more impor- tantly, low manufacturing cost due to its reduced number of active switches. The operating principle of the converter is elaborated; its modulation schemes are discussed. Simulated semiconductor loss analysis and comparison with the back-to-back two-level voltage source converter are presented. Finally, experimental results from a 5-kVA prototype system are provided to verify the validity of the proposed topology.*

***Index Terms*:** *AC/AC converter, pulsewidth modulation (PWM), reduced switch count topology.*

I. INTRODUCTION

THREE-PHASE ac/dc/ac and ac/ac converters with variable frequency (VF) and variable voltage operation have found Wide applications in the industry. The most popular configura- tion uses voltage source inverter (VSI) with a diode rectifier as the front end for adjustable speed drives (ASDs), uninterruptible power supplies (UPS), and other industrial applications [1]. This configuration features low cost and reliable operation due to the use of a diode rectifier, but it generates highly distorted input line currents and does not have regenerative or dynamic braking capability. These problems can be mitigated by using a back-to-back two-level voltage source converter (B2B 2L-VSC), shown in Fig. 1, where a pulsewidth modulation (PWM) voltage source rectifier is used to replace the diode rectifier [2].

The B2B 2L-VSC requires a relatively high number (12) of active switches such as insulated gate bipolar transistors (IG- BTs). It also needs a dc-link capacitor that is responsible for a limited lifespan and increased cost. To reduce the device count and minimize/eliminate the dc-capacitor filter, various converter topologies have been proposed in the literature. The first ap- proach reported in [3]–[5] puts two dc capacitors in cascade

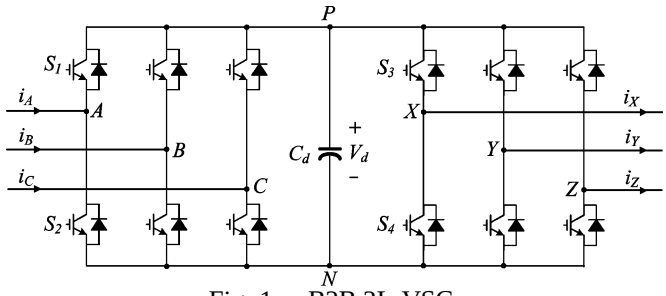

Fig. 1. B2B 2L-VSC.

And takes their midpoint as one of the input–output terminals, whereby an entire phase leg for the rectifier and/or inverter can be saved. It is also possible to reduce the total number of switches, as the second approach suggests [6], [7], by sharing one of the three phase legs between the rectifier and inverter with proper control. In addition, combined use of dc midpoint con- nection and phase leg sharing has been proposed in [8], where only four legs are needed to perform three-phase ac to ac con- version with bidirectional power flow and power factor control. Although all the earlier references achieve the goal of reducing the number of switches and thus reducing the cost, they unexcep- tionally have limits or involve complex control due to their un- balanced topological structure. For unidirectional applications, diodes can be used in place of active switches in the rectifier part, such as the VIENNA rectifier [9], three-phase three-switch buck-type rectifier [10], and three-phase three-switch two-level rectifier [11]. These converters may also be regarded as topolo- gies with a saved number of switches, despite their employment of a large number of diodes.

Unlike VSCs that inevitably require the dc-link stage, the matrix converter [12] presents a radical change in topology and directly converts a fixed ac input voltage to an adjustable ac output voltage. It features sinusoidal input–output, controllable power factor, and is capable of bidirectional energy transfer from the supply to the load or vice versa. Since there is no dc- link circuit, the dc capacitor in the VSC is not necessary here, leading to cost reduction as well as improved reliability and longevity. However, the conventional matrix converter (CMC) normally requires 18 active switches and its switching scheme is complex. The high semiconductor cost and complex control have made this topology less attractive. Similar to the situation of VSCs, efforts to reduce the number of active switches for a matrix converter have been made in recent publications [13], [14], where a couple of topological variants such as the sparse matrix converter (SMC) were proposed. The SMC provides

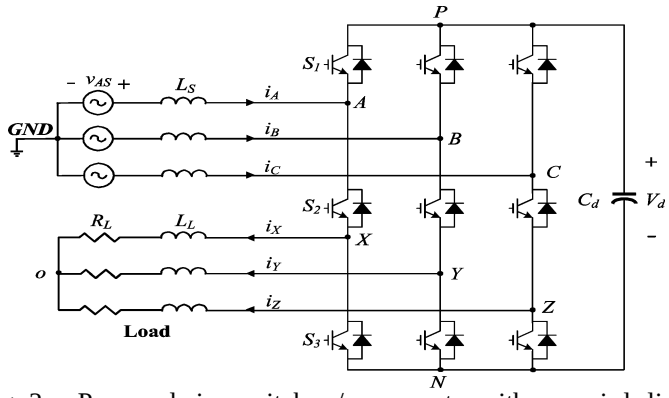

Fig. 2. Proposed nine-switch ac/ac converter with a quasi-dc link.

Equivalent functionality to the CMC. It employs 15 switches with the semiconductor cost still higher than that of the B2B 2 L-VSC. In this paper, a novel one-stage three-phase ac/ac converter topology is proposed. Different from all other existing topolo- gies, this converter has only three legs with only nine active switches for bidirectional ac/ac power conversion.

II. NINE-SWITCH CONVERTER TOPOLOGY

Fig. 2 shows the proposed three-phase nine-switch converter topology. This converter has only three legs with three switches installed on each of them. The novelty herein is that the middle switch in each individual leg is shared by both the rectifier and the inverter, thereby reducing the switch count by 33% and 50% in comparison to the B2B 2L-VSC and CMC, respectively. The input power is delivered to the output partially through the middle three switches and partially through a quasi-dc-link circuit. For the convenience of discussion, we can consider that the rectifier of the nine-switch converter is composed of the top three and middle three switches, whereas the inverter consists of the middle three and bottom three switches.

The converter has two modes of operation: 1) constant fre- quency (CF) mode, where the output frequency of the inverter is constant and also the same as that of the utility supply, while the inverter output voltage is adjustable; and

TABLE I
SWITCHING STATES AND CONVERTER LEG VOLTAGES

(a) Back-to-back converter						
Switching State	S_1	S_2	S_3	S_4	v_{AN}	v_{XN}
1	On	Off	On	Off	V_d	V_d
2	Off	On	Off	On	0	0
3	On	Off	Off	On	V_d	0
4	Off	On	On	Off	0	V_d

(b) Proposed nine-switch converter					
Switching State	S_1	S_2	S_3	v_{AN}	v_{XN}
1	On	On	Off	V_d	V_d
2	Off	On	On	0	0
3	On	Off	On	V_d	0

2) VF mode, where by switches S_1 and S_2 in the rectifier, whereas the inverter leg voltage v_{XN} can be controlled by S_3 and S_4 in the inverter. This means that the rectifier and inverter leg voltages can be controlled independently. The B2B 2L-VSC has four switching states per phase, as defined in Table I.

For the nine-switch topology, the control of the input and out- put voltages has to be accomplished through the three switches on each leg. Because the middle switches are shared by the rectifier and inverter, the proposed converter has only three switching states per phase, as listed in Table I. It can be ob- served that switching state 4 for the B2B 2L-VSC does not exist in the nine-switch converter, which implies that the inverter leg voltage v_{XN} cannot be higher than the rectifier leg voltage v_{AN} at any instant. This is, in fact, the main constraint for the switching scheme design of the nine-switch converter.

Carrier-based continuous PWM schemes for modulating the 2L-VSC, such as sinusoidal PWM (SPWM), space vector PWM (SVPWM), and third-harmonic injection PWM (THIPWM), are well established in the literature [15]. The principles of

these methods can all be applied to the nine-switch converter but a little modification would be necessary, because when designing the switching pattern for the nine-switch converter, the switching constraint discussed earlier must be satisfied.

III. MODULATION SCHEMES

A. Switching Constraint

The reduction of the number of switches in the proposed converter topology imposes certain switching constraints for the switching pattern design. In the B2B 2L-VSC shown in Fig. 1, the rectifier leg voltage v_{AN} , which is the voltage at node A with respect to the negative dc bus N , can be controlled compared with a common triangular carrier v_C . The generated rectifier and inverter leg voltages v_{AN} and v_{XN} are also shown in the figure. This arrangement guarantees that switch state 4 in the B2B 2L-VSC is eliminated here for the nine-switch converter.

B. Modulation Scheme for CF-Mode Operation

Taking SPWM as an example, Fig. 4 illustrates the mod- ified scheme for CF-mode operation, where m_r and m_i are the rectifier and inverter modulation indexes

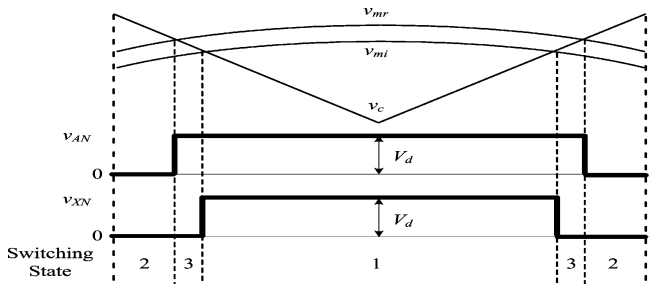

Fig. 3. PWM waveform generation, where switching state 4 of the B2B 2L-VSC is eliminated.

Fig. 3 illustrates the generalized carrier-based modulation scheme in a single switching period for the nine-switch con-both magnitude and frequency of the inverter output voltage are verter. The rectifier modulating wave $v_{m\ r}$ and the inverter modadjustable. The CF-mode operation is particularly suitable for ulating wave $v_{m\ I}$ are arranged such that $v_{m\ r}$ is not lower thanapplications in UPS, whereas the VF mode can be applied to$v_{m\ i}$at any instant of time. These two modulating waveforms are variable-speed drives.

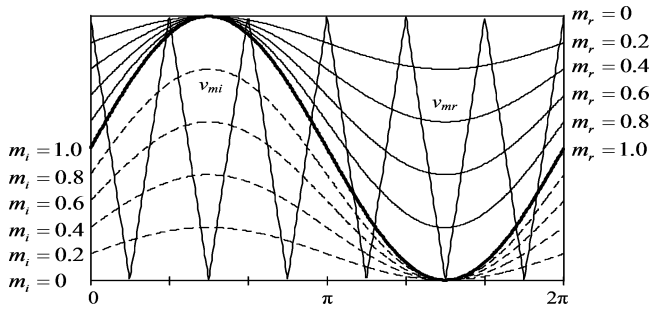

Fig. 4. SPWM scheme for CF-mode operation.

The peak-to-peak magnitude of the sinusoid divided by the peak-to-peak magnitude of the carrier), respectively. The dif- ference between this scheme and the traditional SPWM for 2L-VSC is that here the modulating waves of the rectifier (solid line) and the inverter (dashed line) are placed in a single dc plane and compared to a common triangular carrier wave. The gate signals are generated at the waveforms' intersections with the carrier. To prevent the modulating waves from intersecting each other, the rectifier's modulating waves are lifted to the top of the dc plane whereas the inverter's are pushed to the bottom by adding proper dc offsets. In this way, the switching constraint of the nine-switch converter can be satisfied. In practice, the rectifier side modulation can be synchronized to the grid via a phase-locked loop (PLL). The freedoms of choosing its mod- ulation index m_r and firing angle α between the modulating wave and the grid can be employed to control the dc voltage and the input power factor. The inverter-side modulation index m_i can be freely selected to adjust the output magnitude. If the

inverter's modulating wave is set in phase with the rectifier's, as in the case shown in Fig. 4, both the rectifier and inverter's modulation indexes can simultaneously reach a maximum of unity.

C. Modulation Scheme for VF-Mode Operation

Fig. 5 shows the SPWM modulation scheme for the VF mode of operation. In this case, the inverter's modulation index and

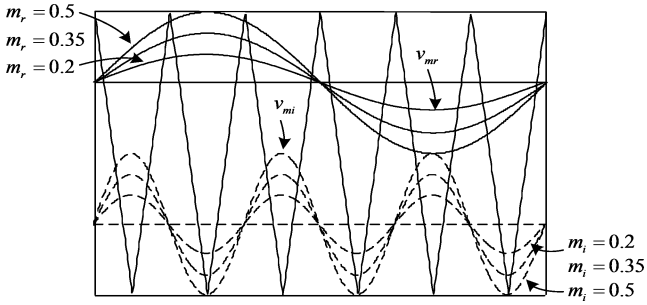

Fig. 5. SPWM scheme for VF-mode operation.

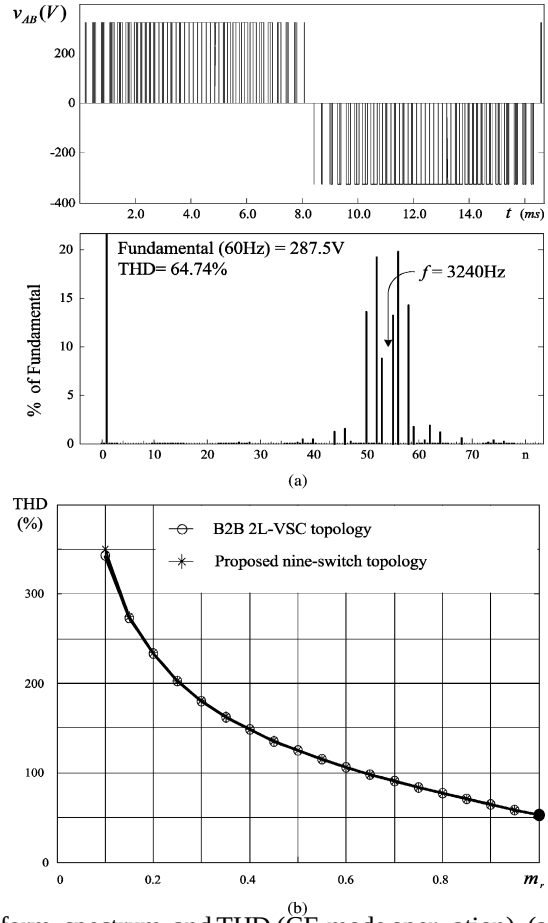

Fig. 6. Rectifier input voltage waveform, spectrum, and THD (CF-mode oper- ation). (a) Rectifier input voltage waveform and spectrum. (b) THD compariso

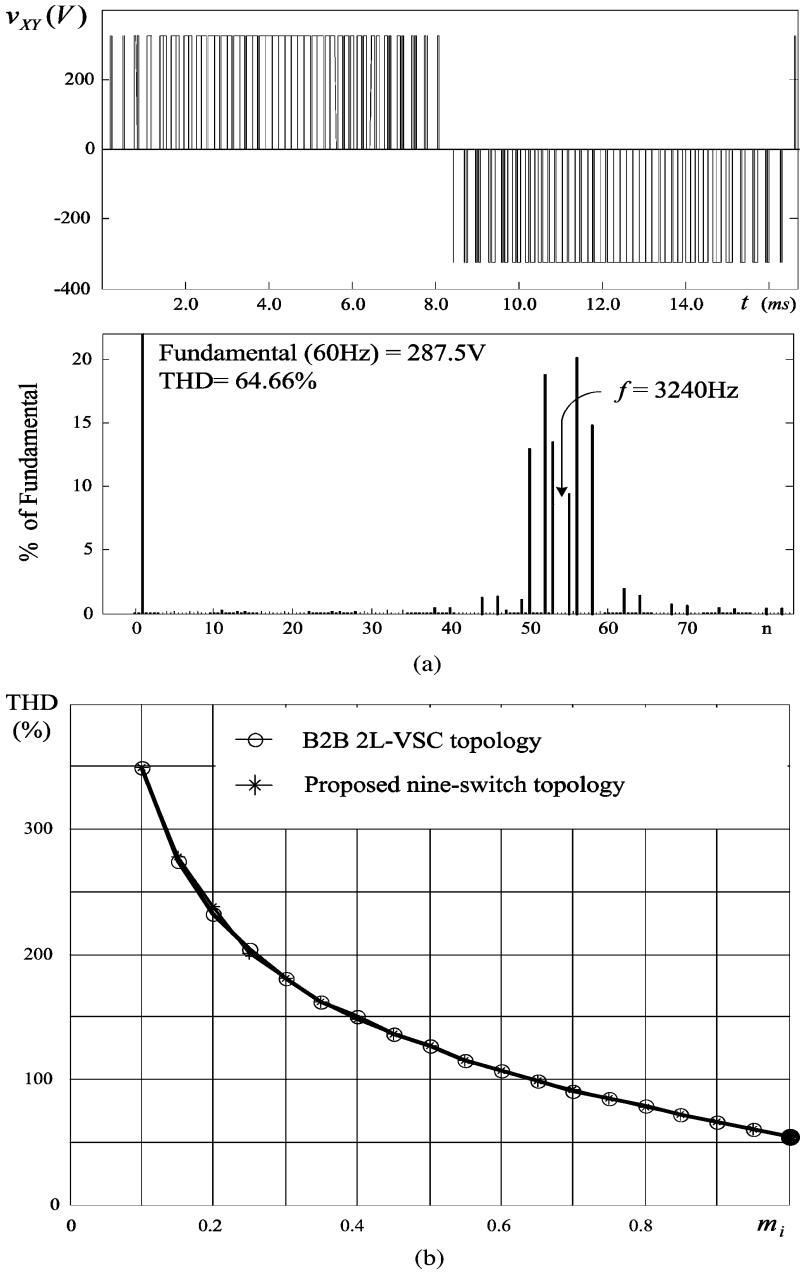

Fig. 7. Inverter output voltage waveform, spectrum, and THD (CF-mode oper- ation). (a) Inverter output voltage waveform and spectrum. (b) THD comparison.

phase angle can both be adjusted independently from the rec- tifier's. In order to satisfy the switching constraint discussed earlier, the sum of the two modulation indexes m_r and m_i of the rectifier and inverter must not exceed 1. For matching the input and output ratings, we limit both of their maximums to 0.5. It can be observed from the figure that both the rectifier and inverter's modulating waves can only be adjusted within half of the carrier's magnitude (which represents the dc volt- age); therefore, the dc voltage v_d of the converter is twice as high as the rated dc voltage of a B2B 2L-VSC with the same ac ratings. This is different from the situation of the CF mode with identical input and output phases, in which the dc voltage of the converter can be tightly controlled and maintained at around its rated value.

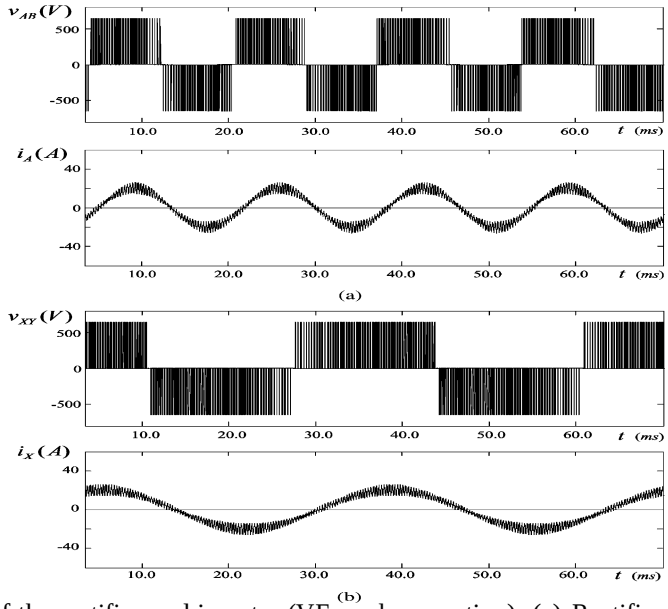

Fig. 8. Simulated waveforms of the rectifier and inverter (VF-mode operation). (a) Rectifier input waveforms at 60 Hz. (b) Inverter output waveforms at 30 Hz.

It should be pointed out that although the added dc offsets guarantee that the instant value of $v_{m\,r}$ is always higher than that of $v_{m\,i}$, they are of zero sequence in the three phases and have no effect on the input/output ac magnitudes. In fact, if the inverter's modulation index is selected to be higher than the rectifier's, e.g., $m_i = 0.5$ and $m_r = 0.2$, the fundamental component of the inverter output voltage v_{XY} will be higher than that of the rectifier input voltage v_{AB}.

IV. SIMULATION ANALYSIS

The performance of the proposed nine-switch converter topol- ogy is simulated with the Matlab/Simulink software. In the sim- ulation, the utility supply is rated at 208 V and 60 Hz with a source inductance of $L_S = 2.5$ mH. The converter is rated at 5 kVA and is driving a three-phase RL load of $R_L = 8\,\Omega$ and $L_L = 2.5$ mH. The dc capacitor C_d is 2350 μF. SVPWM method is used to modulate the converter for its superior performance over SPWM and higher dc voltage utilization. The rectifier is controlled by a vector control scheme with unity power factor operation. The inverter output voltage is not detected, and there- fore, is not tightly controlled. The switching frequency of both

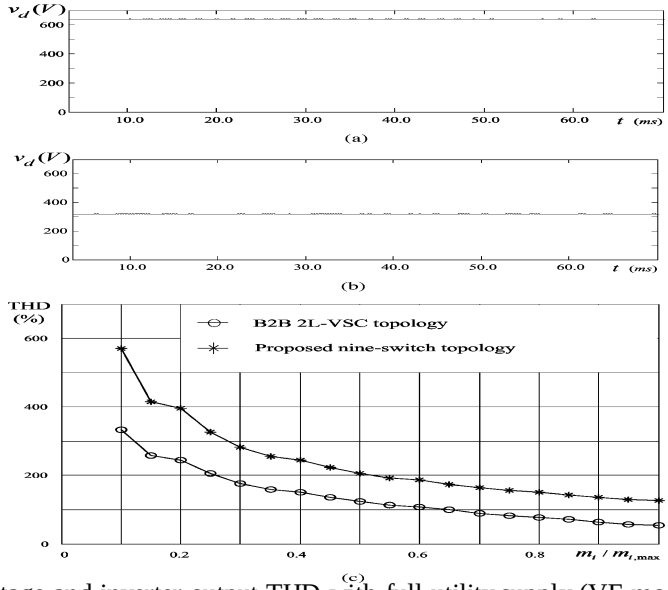

Fig. 9. Comparison of dc voltage and inverter output THD with full utility supply (VF-mode operation). (a) DC voltage of nine-switch converter. (b) DC voltage of B2B 2L-VSC. (c) THD comparison of inverter output.

rectifier and inverter is 3240 Hz. Both CF and VF modes of operation are investigated.

A. CF-Mode Operation

Fig. 6(a) shows the simulated waveform of the rectifier input voltage v_{AB} and its harmonic spectrum with the converter operating in the CF mode. The modulation indexes for the rectifier m_r and inverter m_i are both set at 0.9 and the dc voltage is maintained at 320 V. The frequency of the dominant switching harmonics is centered around 3240 Hz, which is the carrier fre- quency and also the switching frequency of the converter. The low-order harmonics are negligibly small.

Fig. 6(b) illustrates the total harmonic distortion (THD) curve of the rectifier input voltage v_{AB} versus the rectifier modulation index m_r of the nine-switch converter. The THD curve of the input voltage of the B2B 2L-VSC operating at the same switching frequency is also plotted. It can be noted that the harmonic performance of the nine-switch converter is the same as that of its counterpart.

TABLE II
RATED SYSTEM PARAMETERS

	Nine-Switch (CF)	Nine-Switch (VF)	B2B 2L-VSC
Rated dc voltage $V_{d,R}$	320V	640V	320V
Rated IGBT voltage $V_{CE,R}$ / current $I_{C,R}$	600V/50A	1200V/50A	600V/50A
Rated switching power $V_{CE,R}$•$I_{C,R}$•n	270kVA	540kVA	360kVA

TABLE III
INTERPOLATED PARAMETERS FOR LOSS CALCULATION

	600V/50A IGBT BSM50GB60DLC	1200V/50A IGBT BSM50GB120DLC
V_{T0}	1.12	1.55
r_{CE}	0.0218	0.024
V_{D0}	0.8	1.0
r_D	0.0072	0.013
A_{onT}	0	0
B_{onT}	0.0103	0.139
A_{offT}	0.15	1.4
B_{offT}	0.017	0.096
A_{offD}	0.65	1.32
B_{offD}	0.0175	0.047

Fig. 7(a) shows the simulated waveform and spectrum of the inverter output voltage v_{XY} with a fundamental frequency of 60 Hz. It is interesting to note that the inverter output voltage waveform, its fundamental component, and THD are very close to those of the rectifier given in Fig. 6.

Similar to Fig. 6(b), Fig. 7(b) gives the THD comparison of the inverter output voltage v_{XY} between the nine-switch converter and the B2B 2L-VSC, with respect to the inverter modulation index m_i . It can be seen that the inverter out- put THD characteristics are identical to that of the rectifier input.

B. VF-Mode Operation

Fig. 8 shows the simulated rectifier input and inverter output waveforms when the converter operates in the VF mode. The rectifier operates at 60 Hz while the inverter operates at 30 Hz. The modulation indexes for the rectifier and inverter are both 0.45. The figure illustrates that the rectifier and the inverter can operate independently with different fundamental frequencies. Fig. 9(a) and (b) presents the VF-mode dc voltage comparison between the nine-switch converter and the B2B 2L-VSC. Due to the boost nature of the rectifier, the dc voltage v_d of the nine-switch converter in VF mode becomes twice that in the CF mode, which is also the rated value of a B2B 2L-VSC with identical ac ratings. A THD comparison of the inverter output voltage v_{XY} versus the normalized inverter modulation index $m_i / m_{i,\max}$ is shown in Fig. 9(c), where the maximum

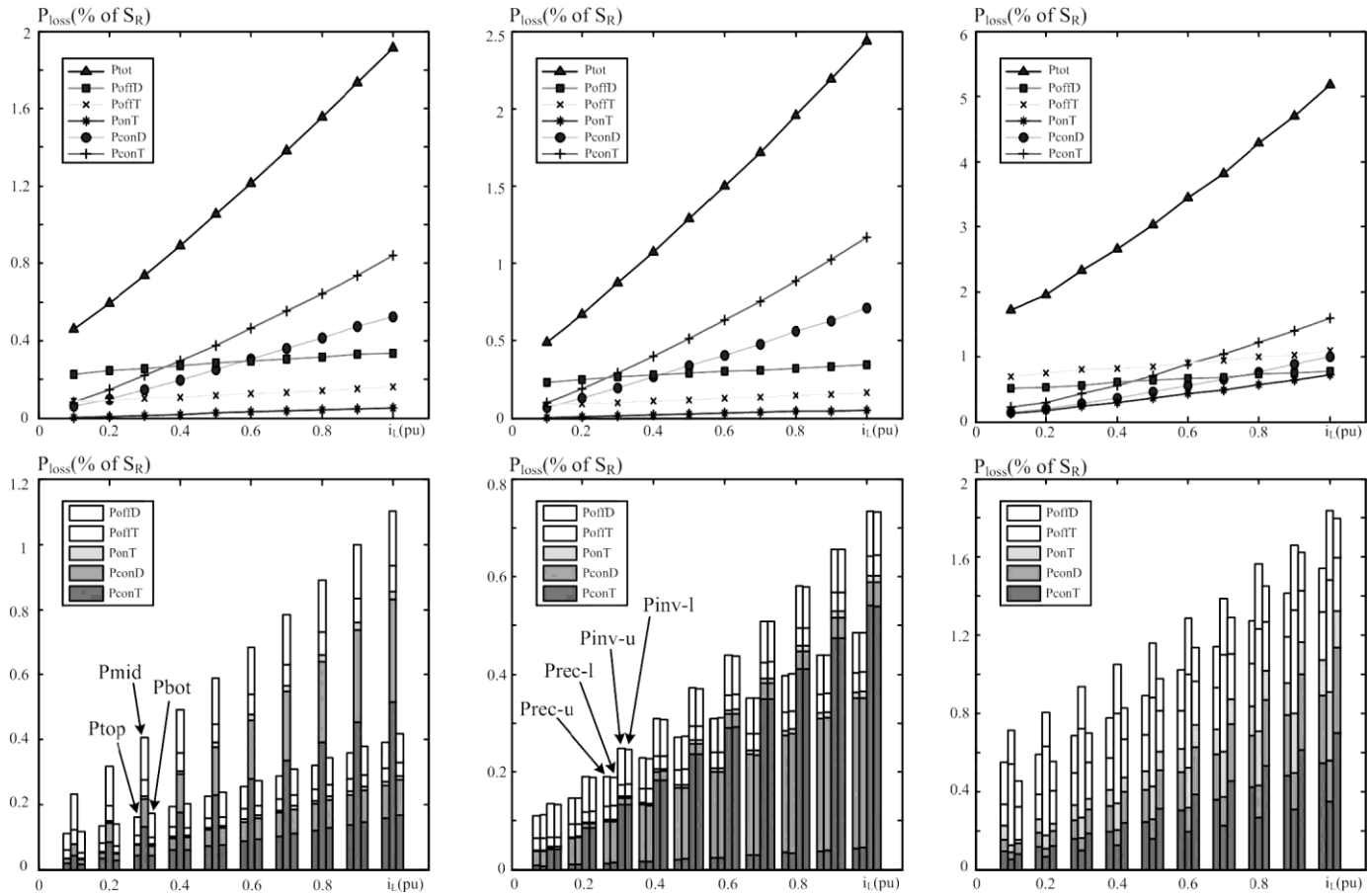

Fig. 10. Semiconductor loss versus load current i_L . (a) Nine-switch converter (CF mode). (b) B2B 2L-VSC. (c) Nine-switch converter (VF mode).

modulation index $m_{i,\max}$ for the nine-device converter and the B2B 2L-VSC are 0.5 and 1, respectively. It can be noted that with the same ac-side voltage magnitudes, the THD of the nine- switch converter output is much higher than that of a competitive B2B 2L-VSC because of the lower modulation index that the nine-switch converter is working at.

V. SIMULATED SEMICONDUCTOR LOSS ANALYSIS

To further study the operating mechanism of the proposed nine-switch converter, it would be necessary to investigate the converter's power loss profile. In this section, a comparative study is presented for the nine-switch converter and the B2B 2 L-VSC. The system parameters and rated switching power of the converters are listed in Table II. For all the converters, the base value of the system power S_R and the source/load side line single switch is used instead. The loss model for the IGBTs incorporated in the simulation is expressed in (1)–(5), where semiconductor losses are abbreviated as $P_{\mathrm{con}T}$ (conduction loss of IGBT), $P_{\mathrm{con}D}$ (conduction loss of diode), $P_{\mathrm{on}T}$ (turn-on loss of IGBT), $P_{\mathrm{off}\ T}$ (turn-off loss of IGBT), and $P_{\mathrm{off}\ D}$ (reverse re- covery loss of diode) [17]. All the losses are averaged over the output fundamental cycle T_1 . Constants such as $V_{T\,0}$, r_{CE}, $A_{\mathrm{on}T}$, and $B_{\mathrm{on}T}$ are derived by linear interpolation from a commer- cial manufacturer's datasheet and are specified in Table III. The accuracy of this model is acceptable provided that the switch- ing and dead time, as well as the switching frequency ripple, is neglected; also, the junction temperature of the switches is assumed constant when the converter's switching frequency is much higher than its input–output frequency voltage are 5 kVA and 208 V. Due to the nine-switch converter's distinctive topological structure, input–output currents flowing through the switches a convenient way to obtain detailed loss information on every

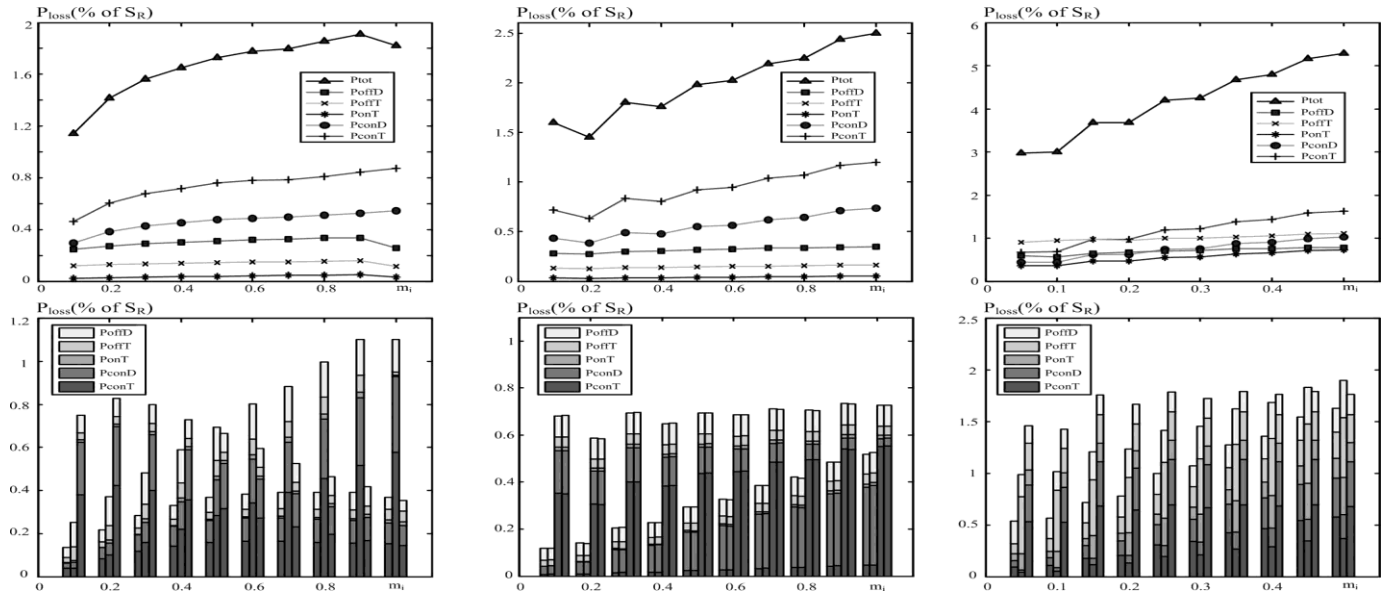

Fig. 11. Semiconductor loss versus output modulation index m_i . (a) Nine-switch converter (CF mode). (b) B2B 2L-VSC. (c) Nine-switch converter (VF mode).

$$P_{\text{off } T}(t)) = \begin{cases} A_{\text{off } T} + B_{\text{off } T} i_c & t \in (t_0, t_0 + T_1] \\ 0 & \text{otherwise} \end{cases} \quad (4)$$

$$P_{\text{off } D} = \frac{\int_{t \in (t_0, t_0 + T_1]} (A_{\text{off } D} + B_{\text{off } D} i_F(t))}{T_1}. \quad (5)$$

loss profile no matter which mode it is in. Therefore, the loss di- agram of the two modes for B2B 2L-VSC is shown in the same figure. Note that the CF-mode nine-switch converter and the B2B 2L-VSC are simulated with the 600-V IGBT parameters,

In order to perform a comparative evaluation, a B2B 2L-VSC with identical power rating is also simulated with the derived loss model. Using the same parameters, modulation and control scheme, and being simulated in the same working conditions, the simulation results can help reveal some of the commonalities and differences between the two converters.

The simulated loss diagrams for the nine-switch converter and the B2B 2L-VSC are shown in Figs. 10 and 11. In addition to the aforementioned individual losses, P_{tot} indicates the total semiconductor loss of the studied converter. For the nine-switch Converter, P_{top}, P_{mid}, and P_{bot} denote losses in the top, middle, and bottom three switches, respectively. For the 2L-VSC, losses on the upper and lower switches in the rectifier and inverter are denoted as $P_{\text{rec-u}}$, $P_{\text{rec-l}}$, $P_{\text{inv-u}}$, and $P_{\text{inv-l}}$. Both converters are simulated in CF and VF mode with system specifications iden- tical to those given in Section IV. However, it was verified from simulation that if parameters other than the output fundamental frequency are not changed, the B2B 2L-VSC keeps the same Whereas the VF-mode nine-switch converter requires the use of the 1200-V IGBT. Switching losses $P_{\text{on}T}$, $P_{\text{off } T}$, and $P_{\text{off } D}$ are proportionally scaled with respect to the converters' operating dc voltages in the simulation.

Fig. 10 shows the losses in both converters as a function of the normalized load current in per unit value (p.u.). The con- verters are operated with unity input power factor, a switching frequency of 3240 Hz, and the inverter modulation index of 0.9. From the figure, it can be seen that the total semiconductor loss of both CF- and VF-mode nine-switch converters follows a sim- ilar trend to the B2B 2L-VSC with respect to the load current change, although the CF-mode loss is always lower than that of the B2B 2L-VSC due to its partial single-stage power transfer nature. Unlike the B2B 2L-VSC that possesses a symmetrical structure, the loss distribution on the top, middle, and bottom switches are not even in the CF-mode nine-switch converter. In general, the middle three switches dissipate more than twice the loss of those from the top three and bottom three switches, which is evident in Fig. 10(a). The VF-mode nine-switch con- verter losses, shown in Fig. 10(c), have a more balanced distri- bution on the switches but are significantly higher than those of

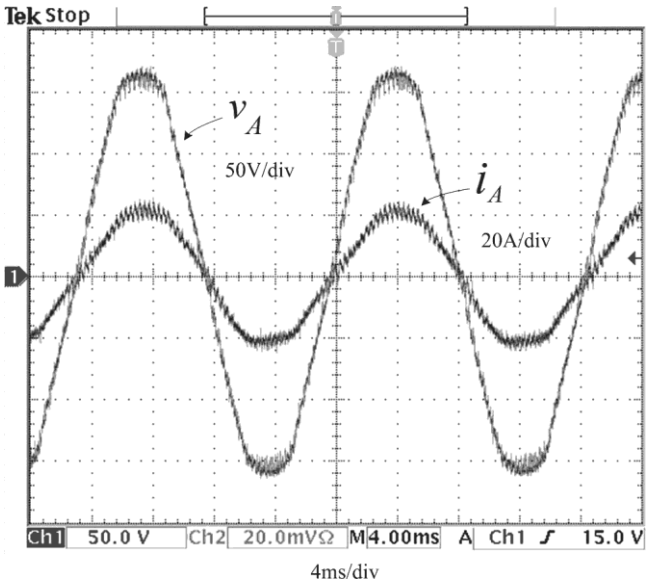

Fig. 12. Unity input power operation of the rectifier.

The B2B 2L-VSC and CF mode nine switch. This is due to its doubled dc voltage and the necessity to use IGBT devices with higher ratings.

In Fig. 11, the changing parameter becomes the converter's output modulation index m_i . A drop of total semiconductor loss can be observed at the end of the curve in Fig. 11(a); this is due to joined pulses at maximum modulation index that leads to reduced times of switchings.

Loss dependency on switching frequency and input and out- put power factors provide similar information, and therefore, are not illustrated here for the sake of brevity.

VI. EXPERIMENTAL VERIFICATION

A 5-kVA prototype system was built and tested. The values of the supply voltage, source inductance L_S , dc capacitor C_d , and *RL* load parameters are the same as those given in the simulation.

A. Unity Power Factor Operation

The input power factor of the converter can be leading, lag- ging, or unity. Fig. 12 shows the measured supply phase voltage v_A and line current i_A of the converter with unity power fac- tor operation. During the test, the dc voltage was maintained at 320 V by the rectifier, and the converter modulation index was $m_r = m_i$ =0.9. It should be noted that the control of the rectifier and inverter is decoupled, and therefore, the inverter operation will not affect the operation of the rectifier.

B. CF-Mode Operation

Fig. 13 shows measured voltage and current waveforms when the inverter operates with the same frequency as that for the rec- tifier. The modulation index of the rectifier and inverter was 0.9, while the dc voltage of the converter was 320 V. The harmonic

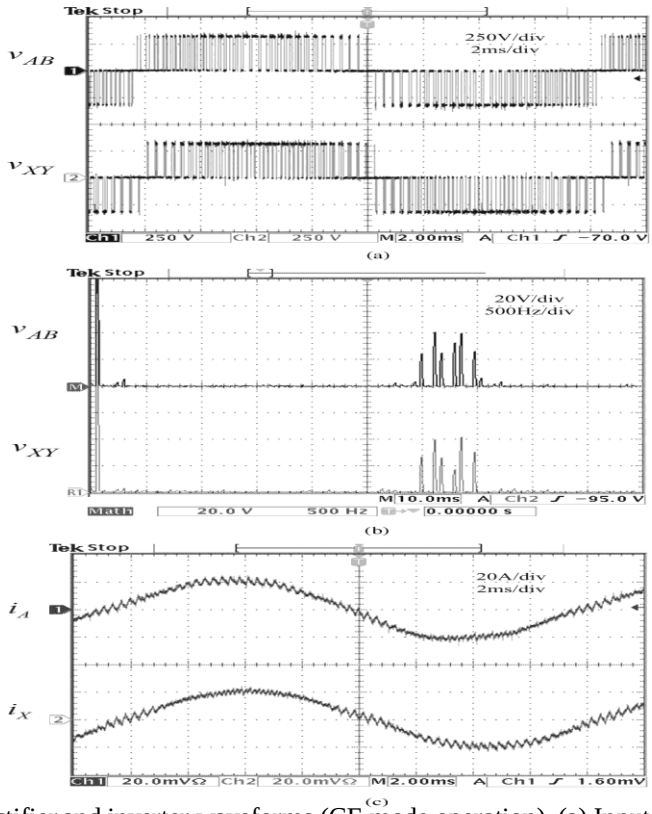

Fig. 13. Measured rectifier and inverter waveforms (CF-mode operation). (a) Input and output voltages. (b) Voltage spectrum. (c) Input and output currents.

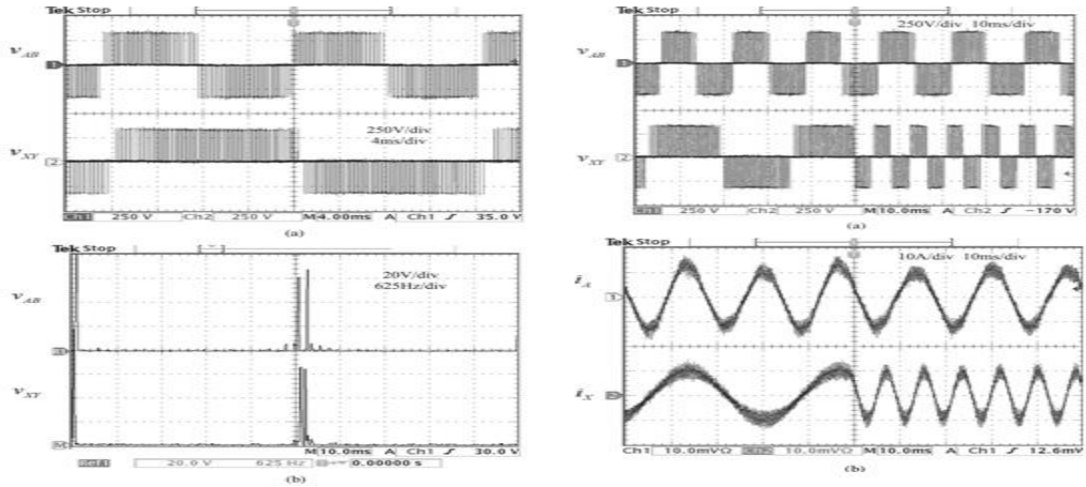

Fig. 14. Measured waveforms and spectrum (VF mode operation). (a) Input and output voltages. (b) Spectrum.

spectrum of v_{AB} and v_{XY} matches very well with the simulation results in Figs. 6 and 7.

C. VF-Mode Operation

Fig. 14 illustrates the converter input and output voltage wave- forms and their harmonic spectrum at the input frequency of 60 Hz and the output frequency of 30 Hz. The modulation index for the rectifier and the inverter is 0.45. The supply voltage in this case is reduced to half of the rated voltage of 208 V such that the dc voltage can remain at 320 V. The spectrum shows that the frequency of the dominant harmonics is centered around 3240 Hz, while all the low-order harmonics are eliminated.

Fig. 15 shows the dynamic response of the converter input and output waveforms when the converter output frequency has a step increase from 30 to 120 Hz. It demonstrates that the control for the converter input and output variables is independent and decoupled, similarly to that of the B2B 2L-VSC.

VII. CONCLUSION

A novel nine-switch PWM ac/ac converter topology was pro- posed in this paper. The topology uses only nine IGBT devices for ac to ac conversion through a quasi dc-link circuit. Com- pared with the conventional back-to-back PWM VSC using 12 switches and the matrix converter that uses 18, the number of switches in the proposed converter is reduced by 33% and 50%, respectively. The proposed converter features sinusoidal inputs and outputs, unity input power factor, and low manufacturing cost. The operating principle of the converter was elaborated, and modulation schemes for constant and VF operations were developed. Simulation results including a semiconductor loss analysis and comparison were provided, which reveal that the proposed converter, while working in CF mode, has an overall higher efficiency than the B2B 2L-VSC at the expense of uneven loss distribution. However, the VF-mode version requires IGBT devices with higher ratings and dissipates significantly higher losses, and thus, is not as attractive as its counterpart. Experi- mental verification is carried out on a 5-kVA prototype system.

REFERENCES

[1] B. Wu, High-power Converters and AC Drives. Piscataway, NJ: IEEE/Wiley, 2006.
[2] B. Singh, B. N. Singh, A. Chandra, K. Al-Haddad, A. Pandey, and D.P. Kothari, "A review of three-phase improved power quality AC– DC converters," IEEE Trans. Ind. Electron., vol. 51, no. 3, pp. 641–660, Jun. 2004.
[3] F. Blaabjerg, S. Freysson, H. H. Hansen, and S. Hansen, "A new op- timized space-vector modulation strategy for a component-minimized voltage source inverter," I E E E Trans. Power Electron., vol. 12, no. 4, pp. 704–714, Jul. 1997.
[4] R. L. A. Ribeiro, C. B. Jacobina, E. R. C. da Silva, and A. M. N. Lima, "AC/AC converter with four switch three phase structures," in Proc. IEEE PESC, 1996, vol. 1, pp. 134–139.
[5] K. Gi-Taek and T. A. Lipo, "VSI-PWM rectifier/inverter system with a reduced switch count," IEEE Trans. Ind. Appl., vol. 32, no. 6, pp. 1331–1337, Nov./Dec. 1996.
[6] A. Bouscayrol, B. Francois, P. Delarue, and J. Niiranen, "Control imple- mentation of a five-leg AC–AC converter to supply a three-phase induction machine," IEEE Trans. Power Electron., vol. 20, no. 1, pp. 107–115, Jan. 2005.
[7] C. B. Jacobina, I. S. de Freitas, E. R. C. da Silva, A. M. N. Lima, and R. L. A. Ribeiro, "Reduced switch count DC-link AC–AC five-leg con- verter," IEEE Trans. Power Electron., vol. 21, no. 5, pp. 1301–1310, Sep. 2006.
[8] C. B. Jacobina, I. S. de Freitas, and A. M. N. Lima, "DC-link three-phase- to-three-phase four-leg converters," IEEE Trans. Ind. Electron., vol. 54, no. 4, pp. 1953–1961, Aug. 2007.
[9] J. Minibock and J. W. Kolar, "Novel concept for mains voltage propor- tional input current shaping of a VIENNA rectifier eliminating controller multipliers," IEEE Trans. Ind. Electron., vol. 52, no. 1, pp. 162–170, Feb. 2005.
[10] T. Nussbaumer, M. Baumann, and J. W. Kolar, "Comprehensive design of a three-phase three-switch buck-type PWM rectifier," IEEE Trans. Power Electron., vol. 22, no. 2, pp. 551–562, Mar. 2007.
[11] F. A. B. Batista and I. Barbi, "Space vector modulation applied to three- phase three-switch two-level unidirectional PWM rectifier," IEEE Trans. Power Electron., vol. 22, no. 6, pp. 2245–2252, Nov. 2007.
[12] P. W. Wheeler, J. Rodriguez, J. C. Clare, L. Empringham, and A. Weinstein, "Matrix converters: A technology review," I E E E Trans. Ind. Electron., vol. 49, no. 2, pp. 276–288, Apr. 2002.
[13] L. Wei, T. A. Lipo, and H. Chan, "Matrix converter topologies with reduced number of switches," in Proc. IEEE PESC, 2002, vol. 1, pp. 57–63.
[14] J. W. Kolar, F. Schafmeister, S. D. Round, and H. Ertl, "Novel three-phase AC–AC sparse matrix converters," IEEE Trans. Power Electron., vol. 22, no. 5, pp. 1649–1661, Sep. 2007.
[15] A. M. Hava, R. J. Kerkman, and T. A. Lipo, "Simple analytical and graphical methods for carrier-based PWM–VSI drives," IEEE Trans. Power Electron., vol. 14, no. 1, pp. 49–61, Jan. 1999.
[16] F. Blaabjerg, U. Jaeger, and S. Munk-Nielsen, "Power losses in PWM–VSI inverter using NPT or PT IGBT devices," IEEE Trans. Power Electron., vol. 10, no. 3, pp. 358–367, May 1995.
[17] Infineon Technologies, Application Note ANIP9931E—Calculation of Major IGBT Operating Parameters. Germany: Infineon Technologies, 1999.

Mr.V.SAMBASIVA RAO was born in 1984. I received B.Tech degree from Jawaharlal Nehru Technological University, Hyderabad in the year 2006. He is presently working as Assistant Lecture in the Department of Electrical and Electronics Engineering at S.E.S.S.N.M POLYTECHNIC, Andhra Pradesh,India.

Mr.M.LOKYA was born in 1984. He graduated from KAKATIYA UNIVERSITY, in the year 2005. He Received M.Tech degree from Jawaharlal Nehru Technological University, Hyderabad in the year 2011. He is presently working as Assistant Professor in the Department of Electrical and Electronics Engineering at Mother Teresa Institute of Science and Technology, Andhra Pradesh,India.

Chalasani Hari Krishna was born in 1982. He graduated from Jawaharlal Nehre Technological University, Hyderabad in the year 2003. He received M.E degree from Satyabama University, Chennai in the year 2005. He presently Associate Professor in the Department of Electrical and Electronics Engineering at Mother Teresa Institute of Science and Technology, India. His research area includes DTC and Drives. He presented 11 research papers in various national and international conferences and journals.His research areas include PWM techniques, DC to AC converters and control of electrical drives